Plagioclase archives of depleted melts in the oceanic crust

David A. Neave[1] and Olivier Namur[2]

[1]Department of Earth and Environmental Sciences, The University of Manchester, M13 9PL Manchester, UK

[2]Department of Earth and Environmental Sciences, KU Leuven, BE-3001 Leuven, Belgium

ABSTRACT

Mid-ocean ridge and ocean island basalts provide vital but incomplete insights into the chemical structure of Earth's mantle. For example, high-anorthite plagioclase carried by these basalts is generally too primitive and incompatible-element depleted to have crystallized from them. Moreover, erupted basalts rarely preserve the strong isotopic and incompatible-element depletions found in some melt inclusions and mantle residua represented by abyssal peridotites. By integrating experimental observations with published analyses of natural crystals and glasses, we demonstrate that high-anorthite plagioclase is in equilibrium with melts generated by high-degree melting of depleted mantle sources. Although such melts seldom erupt, their imprints on crystal and melt inclusion records nonetheless suggest that high-anorthite plagioclase grows from endmember but essentially unexotic magmas. The widespread occurrence of high-anorthite plagioclase in both oceanic basalts and the oceanic crust hence indicates that depleted melts are pervasive in the upper mantle and lower crust despite rarely reaching the surface. Plagioclase archives therefore imply that depleted melts play much a greater role in lower crustal accretion than typically recognized and that the upper mantle may also be more depleted than previously thought.

INTRODUCTION

Mid-ocean-ridge and ocean-island basalts (MORB and OIB respectively; oceanic basalts collectively) offer important windows into the chemical structure of Earth's mantle (Hofmann, 1997; Stracke, 2021). Over billions of years, lithospheric recycling at subduction zones has created chemically, isotopically and lithologically enriched mantle domains that are ultimately reflected in the compositions of erupted basalts (Chase, 1981). Melt extraction over geological time has also created depleted domains that are well documented in abyssal peridotites but absent from erupted records, reflecting the poor preservation of depleted melts during magmatic evolution (Byerly and Lassiter, 2014; Warren, 2016; Neave et al., 2019). Melt inclusions in primitive crystals, which are relatively resistant mixing-induced overprinting, thus provide vital constraints on the chemical and isotopic variability of primitive melts and their mantle sources (Sobolev and Shimizu, 1993; Maclennan, 2008b, 2008a; Stracke et al., 2019). However, whether melt inclusions faithfully reflect the diversity of deep melt compositions remains to be seen. Fortunately, crystals also record information about the melts from which they grow, and as volumetrically significant components of magmas and cumulates may reflect the relative abundances of chemically distinct melts at depth more closely than melt inclusions.

High-anorthite plagioclase ($X_{An} > 0.8$, where X_{An} = molar Ca/(Ca+Na+K)) is often a major constituent of basalts from ocean islands and slow- to intermediate-spreading mid-ocean ridges (Lange et al., 2013), as well as cumulates from ophiolites and the lower oceanic crust (Browning, 1982; Lissenberg et al., 2013). However, such plagioclase crystals are rarely in major-element equilibrium with erupted oceanic basalts (cf. Natland et al., 1983). Moreover, they are often out of isotopic and incompatible-element equilibrium with their host liquids, implying origins from different mantle melt distributions (Halldórsson et al., 2008; Neave et al.,

2014; Nielsen et al., 2020). High-X_{An} plagioclase cannot be reproduced in experiments on MORB starting compositions with realistic volatile contents (Grove et al., 1992; Kohut and Nielsen, 2003), and calculations with the MELTS algorithm indicate that primitive MORBs (MgO > 8 wt.%) typically saturate in plagioclase with $0.75 < X_{An} < 0.80$ (Neave et al., 2019). High-X_{An} plagioclase crystals in oceanic settings are hence thought to grow from high-Ca# melts (where Ca# = molar Ca/(Ca+Na)) that seldom reach the surface (Grove et al., 1992; Neave et al., 2019). Here we integrate observations from natural and experimental systems to explore the origins of high-X_{An} plagioclase crystals in oceanic settings and discuss the role of depleted melts in forming the oceanic crust and acting as a source of crystals in oceanic basalts.

PLAGIOCLASE-LIQUID EQUILIBRIA

The equilibrium exchange of anorthite (An; $CaAl_2Si_2O_8$) and albite (Ab; $NaAlSi_3O_8$) components between liquid and plagioclase is affected by many variables (Namur et al., 2012, and references therein). In summary, equilibrium plagioclase X_{An} correlates positively with melt Ca#, melt Al# (where Al# = molar Al/(Al+Si)), melt H_2O content and temperature, and negatively with pressure. Melt H_2O contents of oceanic basalts are uniformly low when compared with those of arc basalts (Michael, 1995; Koleszar et al., 2009) and exert little influence over equilibrium plagioclase X_{An} in oceanic settings. Conversely, melt Ca# is inextricably linked with equilibrium X_{An} (Bowen, 1913), though the multicomponent character of magmatic liquids means that the exact nature of this relationship depends on both magma composition and intensive conditions. For example, observations from experiments on synthetic analogues of Icelandic lavas at 300 MPa demonstrate that plagioclase saturates at higher melt MgO contents and temperatures, and with higher X_{An} contents, during the crystallization of high-Ca# primitive melts from depleted sources than it does during the crystallization of low-Ca#

primitive melts from enriched sources (Neave et al., 2019). To place these isobaric observations into the polybaric context of crustal magmatism, we performed new crystallization experiments on the same analogues of the high-Ca# Háleyjabunga and low-Ca# Stapafell lavas from the Reykjanes peninsula in Iceland at 100 and 600 MPa (Supplementary Material).

Plagioclase-liquid equilibria at 100 and 600 MPa are summarized in Fig. 1 alongside published equilibria at 300 MPa from Neave et al. (2019). The depleted Háleyjabunga analogue saturates in plagioclase at higher melt MgO contents (and temperatures) than the enriched Stapafell analogue. While isobaric differences in plagioclase saturation conditions between the two starting compositions reflect mantle-derived variability in melt Ca# and Al#, polybaric differences reflect variability in the relative stabilities of plagioclase and clinopyroxene, with plagioclase generally saturating at lower temperatures (and melt MgO contents) when clinopyroxene stability is enhanced at higher pressures (Fig. 1). Equilibrium plagioclase X_{An} also correlates negatively with clinopyroxene stability and therefore pressure. Overall, melt composition, which correlates with intensive conditions as well as source composition, exerts the main control over X_{An}, and high-X_{An} plagioclase is only produced from the high-Ca# Háleyjabunga analogue (up to X_{An} = 0.88 and 0.85 in the products of 100 and 300 MPa experiments, respectively). Importantly, this demonstrates that high-X_{An} plagioclase is produced from known, if highly depleted, oceanic basalt compositions under realistic intensive conditions (cf. Grove et al., 1992; Kohut and Nielsen, 2003). Thus, even if the Háleyjabunga lava is at the limit of erupted compositions (Fig. 3), our findings nonetheless suggest high-X_{An} plagioclase crystals reflect the crystallization of endmember but otherwise unexotic melts derived from depleted mantle sources.

PREDICTING PLAGIOCLASE-LIQUID EQUILIBRIA

By predicting equilibrium plagioclase X_{An} as a function of melt composition it is possible to evaluate plagioclase-liquid equilibria in more systems than could ever be investigated experimentally. While thermodynamic models allow phase relations to be robustly inter- and extrapolated across wide parameter spaces (Ghiorso and Sack, 1995; Holland et al., 2018), empirical models can be more precise when applied within their calibration ranges (e.g., Namur et al., 2012). Moreover, it is possible to avoid making potentially erroneous assumptions about crystallization conditions by calibrating an empirical model that predicts equilibrium X_{An} from melt compositions alone; intensive conditions are implicit in melt compositions.

Performing multiple linear regression through calibration data (n = 98) from experimental studies on basalts from mid-ocean ridges, an oceanic plateau and an ocean island yields the following relationship between plagioclase X_{An} and melt composition (Fig. 2a; r^2 = 0.88; standard error = 0.03; details and sources in the Supplementary Material):

$$X_{An} = 0.92(0.07)\cdot Ca\#_{melt} + 1.63(0.24)\cdot Al\#_{melt} + 0.24(0.05)\cdot(\text{molar } Ca/Al)_{melt} - 0.54(0.06). \quad (1)$$

Test data (n = 36) from experimental studies on basalts from mid-ocean ridges and a continental hotspot with X_{An} ~ 0.6–0.9 are reproduced well by equation 1 (r^2 = 0.92; standard error = 0.02), albeit with a slight offset to lower X_{An}, possibly because of Na loss from some furnace experiments (Fig. 2b; sources in the Supplementary Material).

ORIGINS OF HIGH-ANORTHITE PLAGIOCLASE

High-X_{An} plagioclase has been described in lavas from many mid-ocean ridge segments and ocean islands (e.g., Lange et al., 2013). Here we apply our model to published Icelandic and MORB glass compositions, though our findings are likely to be applicable in dry basaltic settings where fewer compositions have been published. Equilibrium plagioclase X_{An} predicted from Icelandic (n = 190) and MORB (n = 1687) glass compositions collated by Shorttle and

Maclennan (2011) and Gale et al. (2013), respectively, are shown in Fig. 3. Predicted X_{An} contents were also filtered for plagioclase saturation using a stability criterion from Gale et al. (2014) (see Supplementary Material) .

Predicted plagioclase X_{An} correlates broadly with melt MgO content and Ca# in Icelandic and MORB datasets (Figs. 3A and 3B), though high-Ca# melts occur across a wide range of melt MgO contents (8–11 wt.%), highlighting Ca#'s dominant control over equilibrium plagioclase X_{An}. Crucially, some glasses from both datasets return stable high-X_{An} compositions (n = 33 and 22, respectively). Although these glasses are at the limit of natural variability in the case of MORB, their occurrence nonetheless substantiates rare observations of natural high-X_{An} crystals (X_{An} up to 0.89; Natland et al., 1983). Icelandic glasses return higher predicted maximum X_{An} contents than MORB glasses (up to X_{An} = 0.89 and 0.85, respectively), likely reflecting differences in tectonic setting, source composition and mantle temperature.

As well as being associated with high values of melt Ca# at any given melt MgO content (Figs. 3A and 3B), high-X_{An} plagioclase is typically associated with low melt K_2O contents (often <0.1 wt.%; Figs. 3C and 3D), recapitulating the incompatible-element-depleted character of erupted high-X_{An} crystals (Neave et al., 2014; Nielsen et al., 2020). Such high-Ca#, low-K_2O melts are typically generated by shallow melting of depleted sources that have experienced high degrees of prior fractional melting (e.g., Grove et al., 1992; Shorttle and Maclennan, 2011). High-X_{An} plagioclase is also associated with low melt FeO* contents (total Fe as FeO) at any given melt MgO content (Figs 3E and 3F). This is particularly clear for Iceland, where low-FeO* primitive melts (FeO* < 10 wt.%) are predicted to be equilibrium with high-X_{An} plagioclase but high-FeO* primitive melts (FeO* > 10 wt.%) are not expected to be in equilibrium with plagioclase at all (Fig. 3E). The depleted melts from which high-X_{An} plagioclase crystallizes are

thus from dominantly peridotitic sources and have largely escaped contamination by melts from enriched lithologies during ascent (Shorttle and Maclennan, 2011), though rare K_2O-rich melts in equilibrium with high-X_{An} plagioclase represent exceptions that may have interacted with depleted harzburgites (Fig. 3D; Nielsen et al., 2020). We hence argue that high-X_{An} plagioclase crystals are the solid products of depleted melts feasibly derived from depleted residua recorded by some abyssal peridotites (Byerly and Lassiter, 2014; Warren, 2016) that rarely erupt at the surface despite sometimes being found in melt inclusions (Sobolev and Shimizu, 1993; Maclennan, 2008b; Stracke et al., 2019).

WIDESPREAD DEPLETED MELTS AT DEPTH

High-X_{An} plagioclase occurs throughout the oceanic realm (Fig. 4). In Iceland, it is especially well documented in the Eastern Volcanic Zone (Fig. 4A), where isotopically and incompatible-element-depleted high-X_{An} plagioclase may constitute >30 vol.% of basaltic lavas that are otherwise relatively enriched and evolved (Halldórsson et al., 2008). High-X_{An} plagioclase has also been reported from depleted picrites in the Northern Volcanic Zone of Iceland that formed in response to deglaciation-driven decompression (Maclennan et al., 2003). As well as being found throughout Iceland, high-X_{An} plagioclase is also well documented in Galápagos, Réunion and Kerguelen (Fig. 4A), suggesting that incompatible-element-depleted melts with high Ca# are more prevalent beneath ocean islands than implied from enriched OIBs.

High-X_{An} plagioclase crystals have been widely reported in plagioclase-rich MORBs from slow- to intermediate-spreading mid-ocean ridges (Fig. 4B; Lange et al., 2013; Nielsen et al., 2020). With a few notable exceptions (Fig. 4B; Natland et al., 1983), these high-X_{An} contents are found in crystal cores that are out of equilibrium with their carrier liquids, mirroring observations from ocean islands that high-Ca# melts from depleted sources are probably more

widespread at depth than suggested by erupted archives. Indeed, melt inclusion entrapment pressures typically place high-X_{An} plagioclase crystallization near the Moho (Drignon et al., 2018; Bennett et al., 2019).

High-X_{An} plagioclase crystals are found in lower crustal sections of the fast-spreading Samail ophiolite in Oman (Fig. 4C; Browning, 1982), though elevated melt H_2O contents likely affected plagioclase-liquid equilibria in this setting (Koepke et al., 2021). More convincingly, X_{An} ~ 0.8 plagioclase in lower crustal samples from the fast-spreading East Pacific Rise and very-slow-spreading Southwest Indian Ridge suggests that high-Ca# melts occur throughout the global ridge system (Fig. 4D; Dick et al., 2002; Lissenberg et al., 2013). Observations from the East Pacific Rise also illustrate how magmatic processes bias records of chemical variability, with high-X_{An} absent from seafloor lavas but present at depth, presumably as a consquence of filtering by the axial melt lens. The association of high-X_{An} plagioclase with primitive olivine and clinopyroxene in diverse settings indicates that is forms before mixing or reactive porous flow fully overprint signatures from depleted mantle sources (Maclennan, 2008a; Lissenberg et al., 2013).

In line with observations from abyssal peridotites and melt incluions (Byerly and Lassiter, 2014; Stracke et al., 2019), we argue that the global occurrence of high-X_{An} plagioclase demonstrates that depleted melts are widespread at depth. Two key implications of this are that depleted melts are likely to play a much more important role in lower crustal accretion than currently recognized and that the upper mantle may be considerably more depleted than previously thought.

ACKNOWLEDGMENTS

DAN acknowledges support from the Alexander von Humboldt Foundation (Germany) and NERC (UK; NE/T011106/1). ON acknowledges support from the FWO (Belgium) through an Odysseus grant.

REFERENCS CITED

Bennett, E.N., Jenner, F.E., Millet, M.-A., Cashman, K. V., and Lissenberg, C.J., 2019, Deep roots for mid-ocean-ridge volcanoes revealed by plagioclase-hosted melt inclusions: Nature, v. 572, p. 235–239, doi:10.1038/s41586-019-1448-0.

Bowen, N.L., 1913, The melting phenomena of the plagioclase feldspars: American Journal of Science, v. 35, p. 577–599, doi:10.2475/ajs.s4-35.210.577.

Browning, P., 1982, The petrology, geochemistry and structure of the plutonic rocks of the Oman ophiolite: Open University, 404 p., doi:10.21954/ou.ro.0000de14.

Byerly, B.L., and Lassiter, J.C., 2014, Isotopically ultradepleted domains in the convecting upper mantle: Implications for MORB petrogenesis: Geology, v. 42, p. 203–206, doi:10.1130/G34757.1.

Chase, C.G., 1981, Oceanic island Pb: Two-stage histories and mantle evolution: Earth and Planetary Science Letters, v. 52, p. 277–284, doi:10.1016/0012-821X(81)90182-5.

Danyushevsky, L. V., 2001, The effect of small amounts of H_2O on crystallisation of mid-ocean ridge and backarc basin magmas: Journal of Volcanology and Geothermal Research, v. 110, p. 265–280.

Dick, H.J.B. et al., 2002, Primary silicate mineral chemistry of a 1.5-km section of very slow

spreading lower ocean crust: ODP Hole 735B, Southwest Indian Ridge: Proceedings of the Ocean Drilling Program, Scientific Results, v. 176, doi:10.2973/odp.proc.sr.176.001.2002.

Drignon, M.J., Nielsen, R.L., Tepley, F.J., and Bodnar, R.J., 2018, Upper mantle origin of plagioclase megacrysts from plagioclase-ultraphyric mid-oceanic ridge basalt: Geology, v. 47, p. 1–4, doi:10.1130/G45542.1.

Gale, A., Dalton, C.A., Langmuir, C.H., Su, Y., and Schilling, J.G., 2013, The mean composition of ocean ridge basalts: Geochemistry, Geophysics, Geosystems, v. 14, p. 489–518, doi:10.1029/2012GC004334.

Gale, A., Langmuir, C.H., and Dalton, C.A., 2014, The Global Systematics of Ocean Ridge Basalts and their Origin: Journal of Petrology, v. 55, p. 1051–1082, doi:10.1093/petrology/egu017.

Ghiorso, M.S., and Sack, R.O., 1995, Chemical mass transfer in magmatic processes IV. A revised and internally consistent thermodynamic model for the interpolation and extrapolation of liquid-solid equilibria in magmatic systems at elevated temperatures and pressures: Contributions to Mineralogy and Petrology, v. 119, p. 197–212, doi:10.1007/BF00307281.

Grove, T.L., Kinzler, R.J., and Bryan, W.B., 1992, Fractionation of Mid-Ocean Ridge Basalt (MORB), *in* Mantle Flow and Melt Generation at Mid-Ocean Ridges, Geophysical Monograph 71, Washington D.C., American Geophysical Union, p. 281–310.

Halldórsson, S.A., Óskarsson, N., Grönvold, K., Sigurdsson, G., Sverrisdottir, G., and Steinthórsson, S., 2008, Isotopic-heterogeneity of the Thjorsa lava-Implications for mantle

sources and crustal processes within the Eastern Rift Zone, Iceland: Chemical Geology, v. 255, p. 305–316, doi:10.1016/j.chemgeo.2008.06.050.

Hofmann, A.W., 1997, Mantle geochemistry: the message from oceanic volcanism: Nature, v. 385, p. 219–229, doi:10.1038/385219a0.

Holland, T.J.B., Green, E.C.R., and Powell, R., 2018, Melting of peridotites through to granites: a simple thermodynamic model in the system KNCFMASHTOCr: Journal of Petrology, v. 59, p. 881–900, doi:10.1093/petrology/egy048.

Koepke, J., Feig, S.T., Berndt, J., and Neave, D.A., 2021, Wet magmatic processes during the accretion of the deep crust of the Oman Ophiolite paleoridge: Phase diagrams and petrological records: Tectonophysics, v. 8, p. 229051, doi:10.1016/j.tecto.2021.229051.

Kohut, E.J., and Nielsen, R.L., 2003, Low-pressure phase equilibria of anhydrous anorthite-bearing mafic magmas: Geochemistry, Geophysics, Geosystems, v. 4, p. 1–27, doi:10.1029/2002GC000451.

Koleszar, A.M., Saal, A.E., Hauri, E.H., Nagle, A.N., Liang, Y., and Kurz, M.D., 2009, The volatile contents of the Galapagos plume; evidence for H$_{2}$O and F open system behavior in melt inclusions: Earth and Planetary Science Letters, v. 287, p. 442–452, doi:10.1016/j.epsl.2009.08.029.

Lange, A.E., Nielsen, R.L., Tepley, F.J., and Kent, A.J.R., 2013, The petrogenesis of plagioclase-phyric basalts at mid-ocean ridges: Geochemistry, Geophysics, Geosystems, v. 14, p. 3282–3296, doi:10.1002/ggge.20207.

Lissenberg, C.J., MacLeod, C.J., Howard, K.A., and Godard, M., 2013, Pervasive reactive melt migration through fast-spreading lower oceanic crust (Hess Deep, equatorial Pacific Ocean): Earth and Planetary Science Letters, v. 361, p. 436–447, doi:10.1016/j.epsl.2012.11.012.

Maclennan, J., 2008a, Concurrent mixing and cooling of melts under Iceland: Journal of Petrology, v. 49, p. 1931–1953, doi:10.1093/petrology/egn052.

Maclennan, J., 2008b, Lead isotope variability in olivine-hosted melt inclusions from Iceland: Geochimica et Cosmochimica Acta, v. 72, p. 4159–4176, doi:10.1016/j.gca.2008.05.034.

Maclennan, J., McKenzie, D., Grönvold, K., Shimizu, N., Eiler, J.M., and Kitchen, N., 2003, Melt mixing and crystallization under Theistareykir, northeast Iceland: Geochemistry, Geophysics, Geosystems, v. 4, p. 1–40, doi:10.1029/2003GC000558.

Michael, P.J., 1995, Evidence from trace elements and H_2O for regionally distinctive sources of depleted MORB: Implications for evolution of the depleted mantle: Earth and Planetary Science Letters, v. 131, p. 301–320, doi:10.1180/minmag.1994.58A.2.52.

Namur, O., Charlier, B., Toplis, M.J., and Vander Auwera, J., 2012, Prediction of plagioclase-melt equilibria in anhydrous silicate melts at 1-atm: Contributions to Mineralogy and Petrology, v. 163, p. 133–150, doi:10.1007/s00410-011-0662-z.

Natland, J.H., Adamson, A.C., Laverne, C., Melson, W.G., and O'Hearn, T., 1983, A Compositionally Nearly Steady-State Magma Chamber at the Costa Rica Rift: Evidence from Basalt Glass and Mineral Data, Deep Sea Drilling Project Sites 501, 504, and 505, *in* Initial Reports of the Deep Sea Drilling Project, 69, v. 53, p. 1689–1699,

doi:10.2973/dsdp.proc.69.154.1983.

Neave, D.A., Maclennan, J., Hartley, M.E., Edmonds, M., and Thordarson, T., 2014, Crystal storage and transfer in basaltic systems: the Skuggafjöll eruption, Iceland: Journal of Petrology, v. 55, p. 2311–2346, doi:10.1093/petrology/egu058.

Neave, D.A., Namur, O., Shorttle, O., and Holtz, F., 2019, Magmatic evolution biases basaltic records of mantle chemistry towards melts from recycled sources: Earth and Planetary Science Letters, v. 520, p. 199–211, doi:10.1016/j.epsl.2019.06.003.

Nielsen, R.L., Ustunisik, G., Lange, A.E., Tepley, F.J., and Kent, A.J.R., 2020, Trace Element and Isotopic Characteristics of Plagioclase Megacrysts in Plagioclase Ultraphyric Basalts (PUB): Geochemistry, Geophysics, Geosystems, v. 21, p. 1–24, doi:10.1029/2019GC008638.

Shorttle, O., and Maclennan, J., 2011, Compositional trends of Icelandic basalts: Implications for short-length scale lithological heterogeneity in mantle plumes: Geochemistry, Geophysics, Geosystems, v. 12, p. 1–32, doi:10.1029/2011GC003748.

Sobolev, A. V., and Shimizu, N., 1993, Ultra-depleted primary melt included in an olivine from the Mid-Atlantic Ridge: Nature, v. 363, p. 151–154, doi:10.1038/363151a0.

Stracke, A., 2021, A process-oriented approach to mantle geochemistry: Chemical Geology, v. 184, p. 120350, doi:10.1016/j.chemgeo.2021.120350.

Stracke, A., Genske, F., Berndt, J., and Koornneef, J.M., 2019, Ubiquitous ultra-depleted domains in Earth's mantle: Nature Geoscience, v. 12, p. 851–855, doi:10.1038/s41561-019-

0446-z.

Warren, J.M., 2016, Global variations in abyssal peridotite compositions: Lithos, v. 248–251, p. 193–219, doi:10.1016/j.lithos.2015.12.023.

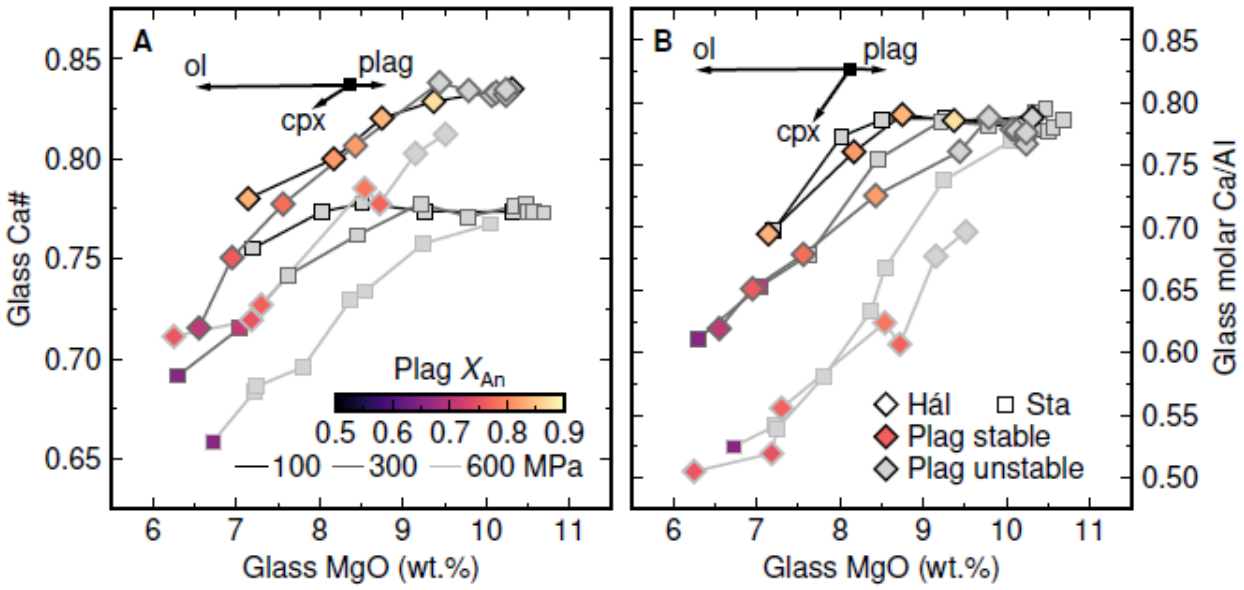

Figure 1. Plagioclase-liquid equilibria in synthetic analogues of the depleted Háleyjabunga (Hál) and enriched Stapafell (Sta) lavas from Iceland summarized in terms of glass MgO content versus (A) glass Ca# (where Ca# = molar Ca/(Ca+Na)) and (B) glass molar Ca/Al. New results at 100 and 600 MPa are presented with results at 300 MPa from Neave et al. (2019). Plagioclase crystallizes earlier and with a higher anorthite content (X_{An}, where X_{An} = molar Ca/(Ca+Na+K)) from high-Ca# depleted melts than low-Ca# enriched melts. Vectors show the crystallization of 5 wt.% equilibrium olivine (ol), clinopyroxene (cpx) and plagioclase (plag) according to the models of Danyushevsky (2001).

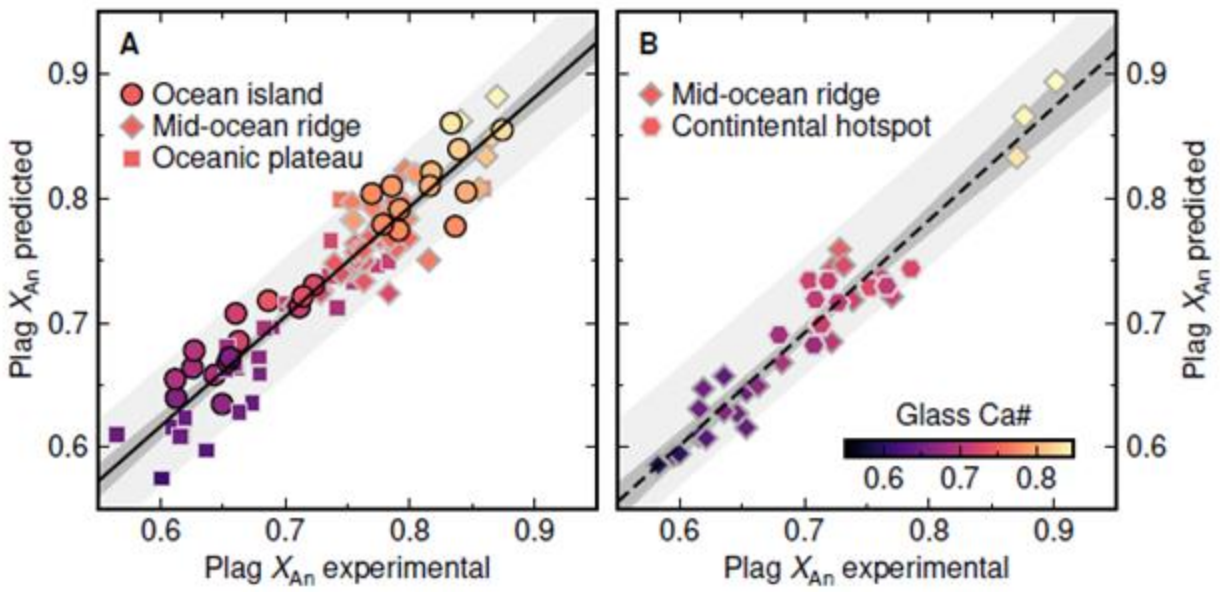

299 Figure 2. (A) Performance of the multiple linear regression (Eq 1) used to predict plagioclase
300 (plag) anorthite content (X_{An}, where X_{An} = molar Ca/(Ca+Na+K)) as a function melt
301 composition. The black line shows a regression through calibration data from experimental
302 studies on basalts from an ocean island, mid-ocean ridges and an oceanic plateau. Dark and pale
303 grey envelopes show 95% confidence and prediction intervals, respectively. (B) Performance of
304 Eq 1 on experimental basalt test data from mid-ocean ridges and a continental hotspot. The
305 dashed black line and dark grey envelope show a regression through the test data and its 95%
306 confidence interval, respectively; the pale grey envelope shows the 95% prediction interval of
307 Eq 1. Data sources in the Supplementary Material.
308

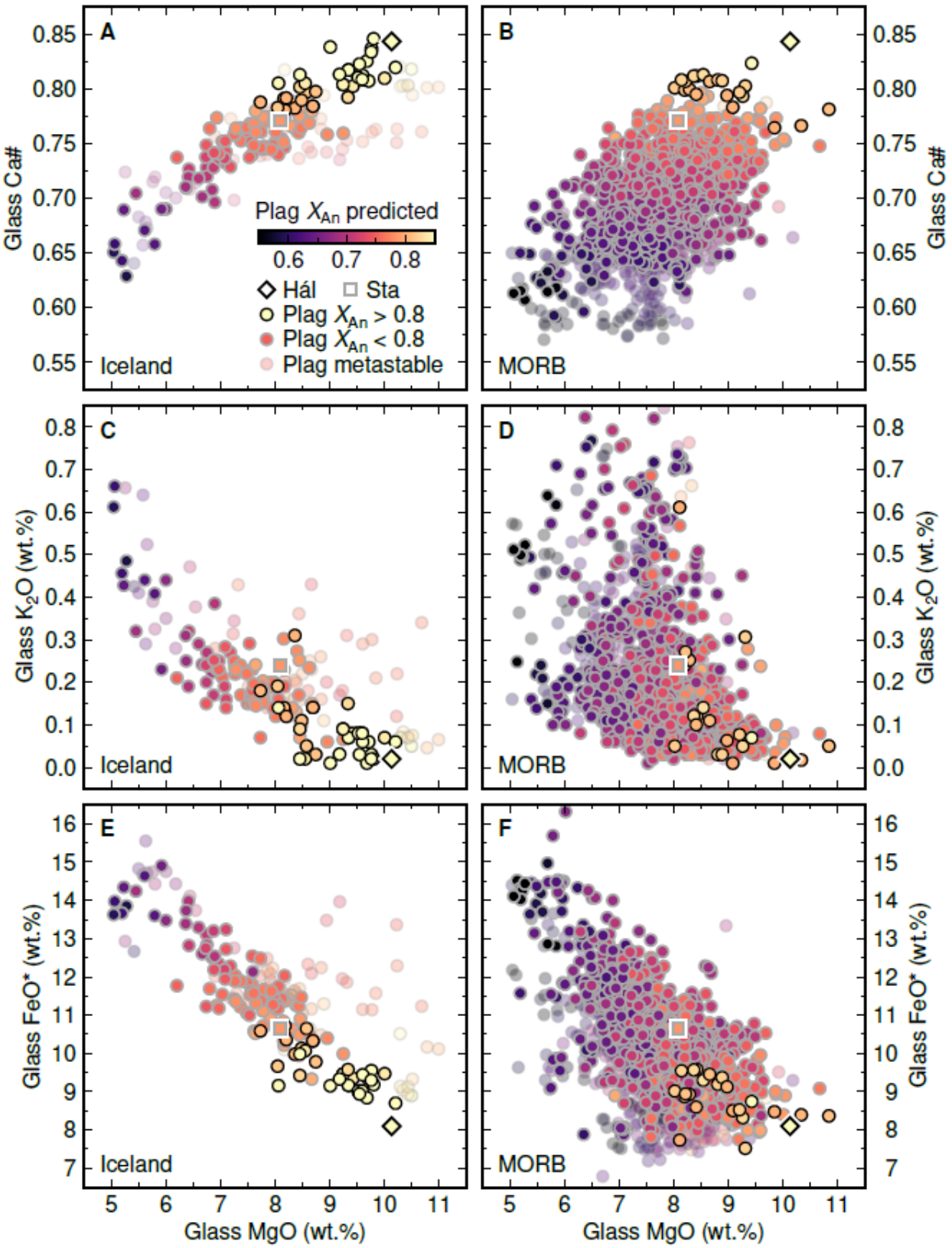
A
B
C
D
E
F
Iceland
MORB
Glass Ca#
Glass K_2O (wt.%)
Glass FeO* (wt.%)
Glass MgO (wt.%)
Plag X_{An} predicted
0.6 0.7 0.8
Hál
Sta
Plag X_{An} > 0.8
Plag X_{An} < 0.8
Plag metastable

309

Figure 3 (previous page). Plagioclase (plag) anorthite contents (X_{An}, where X_{An} = molar Ca/(Ca+Na+K) predicted to be in equilibrium with Icelandic (A, C and E) and MORB (B, D and F) glasses from Shorttle and Maclennan (2011) and Gale et al. (2013), respectively. The evolution of glass compositions is shown for elements emphasizing fractionation (MgO), degree of enrichment (K_2O and FeO*) and control on plagioclase-liquid equilibria (Ca#, where Ca# = molar Ca/(Ca+Na)). Glass compositions that do not pass the plagioclase stability criterion from Gale et al. (2014) are greyed out and those in equilibrium with high-X_{An} plagioclase ($X_{An} > 0.8$) are emphasized with black outlines; Háleyjabunga (Hál) and Stapafell (Sta) glasses are highlighted.

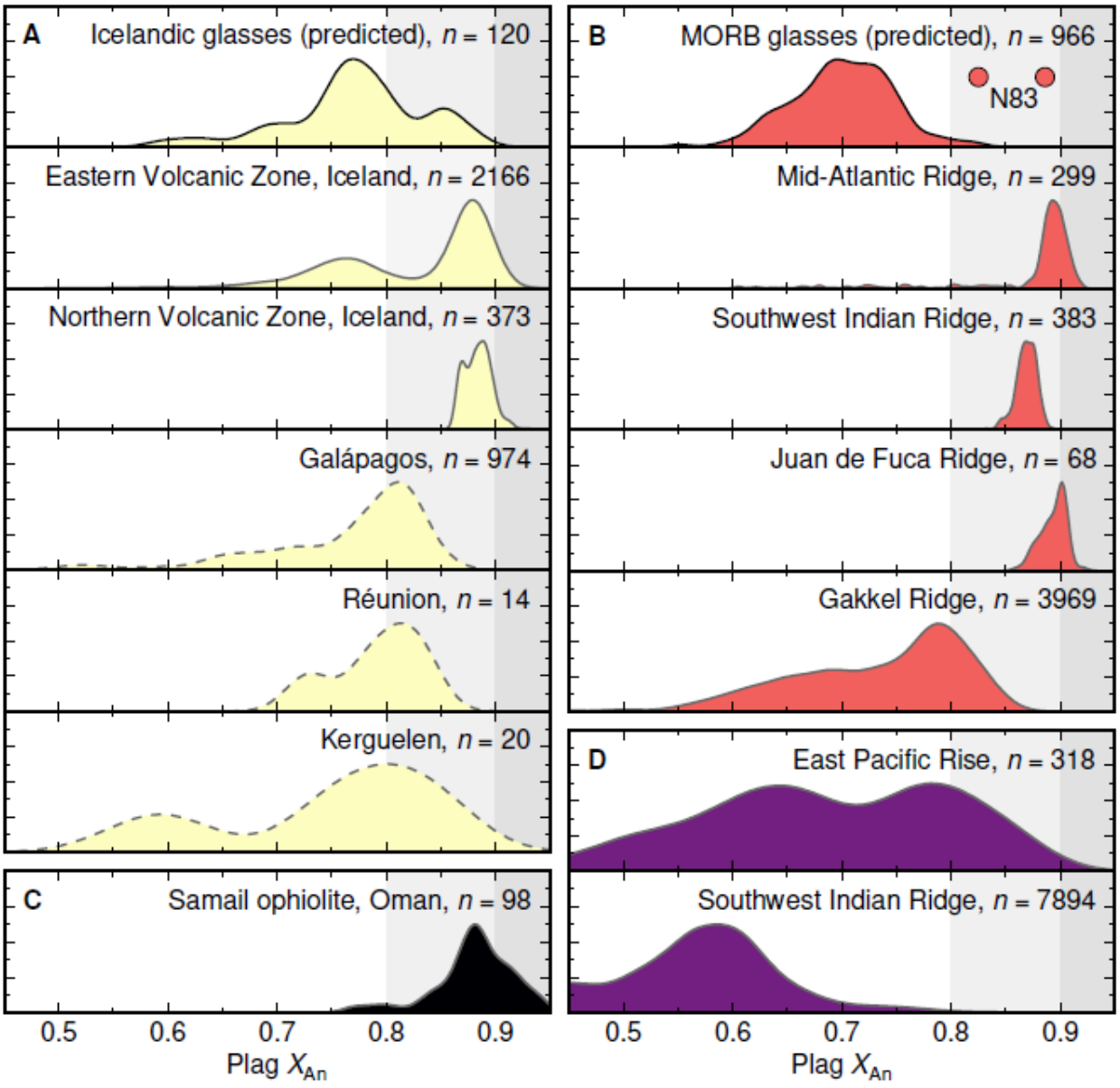

Figure 4. Kernel density estimates summarizing how plagioclase (plag) anorthite contents (X_{An}, where X_{An} = molar Ca/(Ca+Na+K) predicted to be in equilibrium with (A) Icelandic and (B) MORB glasses from Shorttle and Maclennan (2011) and Gale et al. (2013), respectively, compare with natural plagioclase compositions from (A) ocean island basalts, (B) mid-ocean ridge basalts (MORB), (C) the Semail ophiolite, Oman, and (D) the lower oceanic crust. Rare high-X_{An} rims from MORB are highlighted (Natland et al., 1983; N83). Data sources in the Supplementary Material.

Plagioclase archives of depleted melts in the oceanic crust Supplementary Material

David A. Neave[1] and Olivier Namur[2]

[1]Department of Earth and Environmental Sciences, The University of Manchester, M13 9PL Manchester, UK
[2]Department of Earth and Environmental Sciences, KU Leuven, BE-3001 Leuven, Belgium

PHASE EQUILIBRIA EXPERIMENTS

Starting materials

The Háleyjabunga and Stapafell lavas are amongst the most geochemically extreme primitive basalts from Iceland in terms of their major element, trace element and isotopic compositions, which makes them excellent model systems for exploring the consequences of mantle-derived chemical variability (Gurenko and Chaussidon, 1995; Maclennan, 2008). The lavas are thought originate from lithologically distinct mantle sources, with the incompatible-element-depleted Háleyjabunga lava being generated by high-degree melting of an initially fertile peridotite and the Stapafell lava being largely generated by modest-degree melting of a recycled and modally enriched (i.e., clinopyroxene-rich) peridotite (Shorttle and Maclennan, 2011; Neave et al., 2018). Of key relevance here is that the Háleyjabunga lava is relatively Ca- and Al-rich while the Stapafell lava is relatively Fe- and Na-rich, which results in fundamentally different phase equilibria between the two compositions (Neave et al., 2019b).

The synthesis of starting materials is described in detail by Neave et al. (2019b) and summarized below. Natural glass compositions from Condomines et al. (1983), Gurenko and Chaussidon (1995) and Peate et al. (2009) were corrected to the same initial melt MgO content of ~10.5 wt.%. Starting materials with these corrected compositions were then synthesized from reagent-grade oxide and carbonate powders that were fused twice in Pt crucibles at 1600 °C at the Institut für Mineralogie of the Leibniz Universität Hannover, Germany. Platinum crucibles were quenched in H_2O after each fusion to ensure the production of homogenous glasses.

Experimental methods

Crystallization experiments were performed in an internally heated pressure vessel (IHPV) at the Institut für Mineralogie of the Leibniz Universität Hannover, Germany, using methods described in detail by Husen et al. (2016) and Neave et al. (2019b) and summarized below. Approximately 50 mg of each powdered starting material was loaded into $Au_{80}Pd_{20}$ capsules that had first been treated to contain 0.25–0.30 wt.% Fe to minimize Fe exchange with capsule materials (e.g., Gaetani and Grove, 1998). Capsules were suspended from a Pt wire in the hot zone of the IHPV. Experiments were performed at either 100 MPa or 600 MPa in an Ar pressure medium, and at temperatures that ranged from 1140 to 1240 °C. Pressure was monitored with a strain gauge manometer and did not vary by more than 5 MPa during the

course of the experiments. Temperature was monitored with four unsheathed S-type thermocouples spaced across the hot zone and was typically within 5 °C of the target temperature. Experimental temperatures were approached by heating the furnace from room temperature to 10 °C below the target temperature at a rate of 50 °C/min; final heating was performed at a rate of 10 °C/min to avoid overshooting. Experimental durations varied from 48 hours for near- and super-liquidus experiments to 120 hours for lower-temperature experiments. Experimental products were quenched by fusing the Pt wires on which capsules were suspended, thereby dropping them into a cold zone at the base of the vessel.

Analytical methods

The major element content of experimental products was determined by electron probe microanalysis (EPMA) with a Cameca SX100 instrument at the Institut für Mineralogie of the Leibniz Universität Hannover, Germany. Silicon, Ti, Al, Cr, Fe, Mn, Mg, Ca, Na, K and P were measured in glasses with a beam size of 10 µm, an accelerating voltage of 15 kV and a current of 10 nA. Silicon, Ti, Al, Cr, Fe, Mn, Mg, Ca, Na and K were measured in minerals with a beam size of 1 µm, an accelerating voltage of 15 kV and a current of 15 nA. Gold, Pd and Fe were measured in capsules with a beam size of 1 µm, an accelerating voltage of 15 kV and a current of 40 nA. Elements were counted on peak for 20 s, with the exceptions of Si and Na that were counted on peak for 10 s to minimize drift and Na migration. Background counting times were half on-peak counting times. The following standards were used for calibration: wollastonite (Si and Ca), TiO_2 (Ti), Al_2O_3 (Al), Cr_2O_3 (Cr), Fe_2O_3 (for Fe in silicates and Cr-spinel), Fe metal (for Fe in capsules), Mn_3O_4 (Mn), MgO (Mg), albite (Na), orthoclase (K), apatite (P), Au metal (Au) and Pd metal (Pd).

To ensure internal consistency across multiple sessions, analyses were normalized as follows: glass analyses were normalized to VG-2 basalt glass (NMNH 111240-52; using the preferred MgO content); clinopyroxene, low-Ca pyroxene and plagioclase analyses were normalized to Kakanui augite (NMNH 122142; using preferred values); olivine analyses were normalized to San Carlos olivine (NMNH 111312-44); and chromite analyses were normalized to Tiebaghi Mine chromite (NMNH 117075) (Jarosewich et al., 1980). Accuracy and precision were monitored by measuring the following standards that were also normalized for each analytical session: A-99 basaltic glass (NMNH 113498), Ney County Cr-augite (NMNH 164905) and Lake County plagioclase (NMNH 115900) (Jarosewich et al., 1980, 1987). Major (>1 wt.%) and minor (<1 wt.%) elements were determined with accuracies better than 2% and 10%, and 1σ precisions better than 2% and 15% respectively. Analyses of standards are provided alongside analyses of experimental products in the Supplementary Data. Compositions of experimentally produced glasses and plagioclase crystals are summarized in Supplementary Fig. 1.

Glass H_2O contents were determined in experimental products with low crystal contents by Fourier-transform infrared (FTIR) spectroscopy with a Bruker IFS88 instrument at the Institut für Mineralogie of the Leibniz Universität Hannover, Germany, following the methods described by Husen et al. (2016). In short, H_2O contents were determined in ~100-µm thick wafers using the peak attributed to the OH stretch vibration (3550 cm^{-1}) using a molar absorption coefficient

of 68 L/mol cm. Measured glass H_2O contents varied from 0.45 to 0.91 wt.%; all analyses are provided in the Supplementary Data.

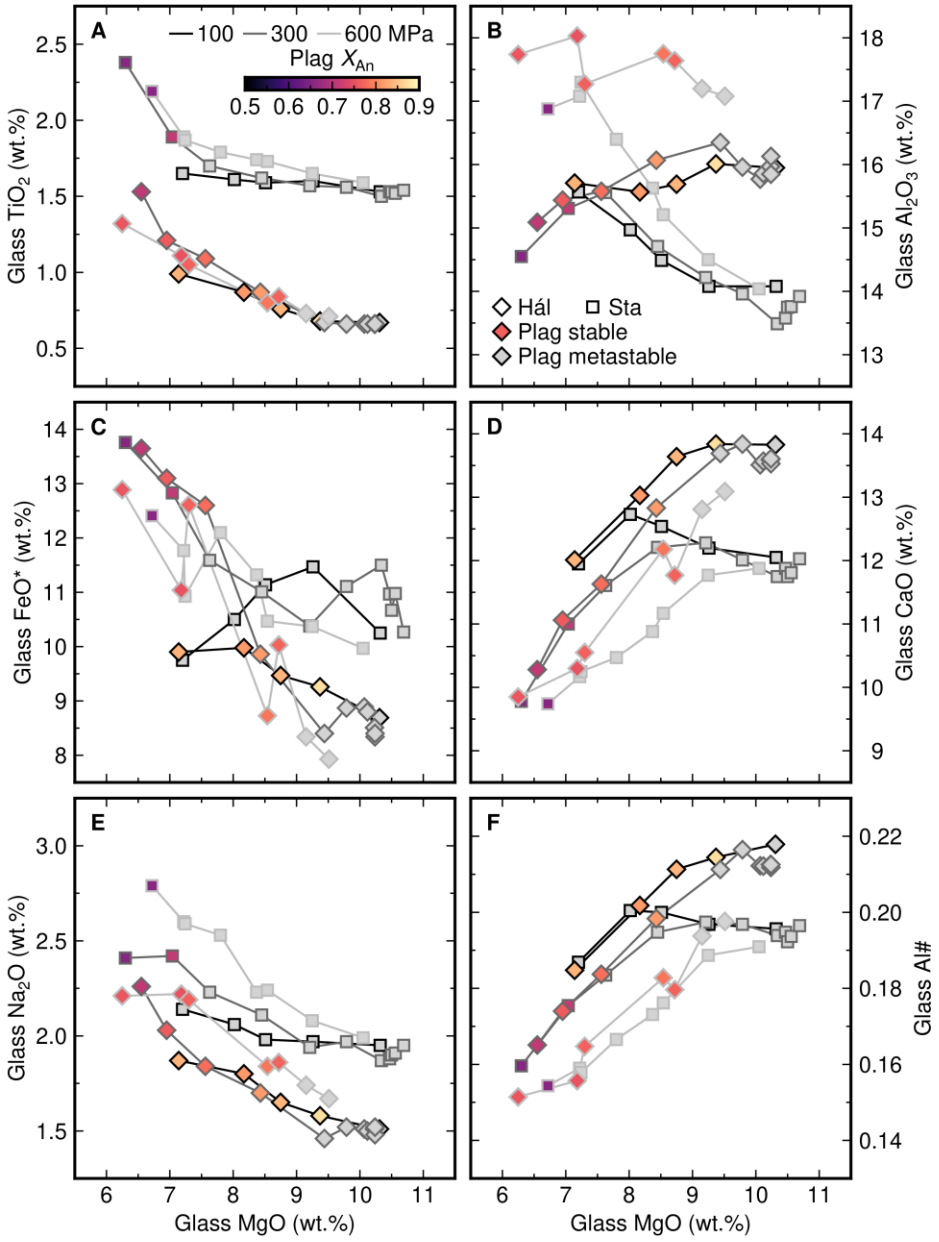

Supplementary Figure 1 Plagioclase-liquid equilibria in synthetic analogues of the depleted Háleyjabunga (Hál) and enriched Stapafell (Sta) lavas from Iceland summarized in terms of glass MgO content versus (A–E) a range of glass major element contents and (F) glass Al# (where Al# = molar Al/(Al+Si)); Fig. 1 in the main text shows equivalent plots for glass Ca# (where Ca# = molar Ca/(Ca+Na)) and glass molar Ca/Al. New results at 100 and 600 MPa are presented alongside results at 300 MPa from Neave et al. (2019b).

Experimental oxygen fugacities

All experiments were conducted under nominally dry conditions (no H_2O was added to dried starting materials), which resulted in melt H_2O contents of 0.56–0.91 wt.% following the reduction of Fe_2O_3 in the starting glasses to FeO and the inward diffusion of trace H_2 from the Ar pressure medium at high temperatures. Colorimetric analyses of experimental products with low crystal contents performed with the approach of Schuessler et al. (2008) returned $Fe^{3+}/\Sigma Fe$ values of 0.13–0.23, which correspond to oxygen fugacity(fO_2) conditions expressed with respect to the fayalite-magnetite-quartz (FMQ) buffer of FMQ+0.2 to FMQ+1.3 (Kress and Carmichael, 1991). Capsule compositions record broadly similar conditions of FMQ+0.0 to FMQ+1.2 (Barr and Grove, 2010). Estimated fO_2 conditions are provided in the Supplementary Data.

PREDICTING PLAGIOCLASE-LIQUID EQUILIBRIA

Rationale and data sources

Empirical models for predicting plagioclase-liquid equilibria and equilibrium plagioclase anorthite contents (X_{An}, where X_{An} = molar Ca/(Ca+Na+K)) are typically calibrated across large ranges of melt composition (Namur et al., 2012 and references therein). While such global calibrations facilitate internally consistent modelling across diverse situations they can also result in lower accuracy and precision than can be achieved by calibrating and applying models under more restricted conditions. Moreover, for technical reasons, the majority of published phase equilibria experiments have been performed at 0.1 MPa (i.e., 1 atm), meaning that plagioclase-liquid equilibria models are generally better constrained at pressures lower than those at which the majority of crustal magmatism takes place (Namur et al., 2012). Here we present a new empirical model optimized for predicting plagioclase-liquid equilibria in oceanic basalts evolving under crustal pressure and temperature conditions.

Calibration data (n = 98) were sourced from relatively recent studies on H_2O-poor (typically <1 wt.%) oceanic tholeiites at a range of pressures (0.1–700 MPa) that report high quality EPMA data. Specifically, data were sourced from experiments on ocean island basalts (OIBs) from Iceland (Neave et al., 2019a, 2019b; this study), mid-ocean-ridge basalts (MORBs) and plagioclase-saturated MORB liquids (Kohut and Nielsen, 2003; Voigt et al., 2017), and oceanic plateau basalts from Shatsky Rise (Husen et al., 2016). Only data from experimental runs containing <50 wt.% glass were used in the calibration to ensure that plagioclase and liquid pairs had approached equilibrium as closely as reasonably possible. The distribution of plagioclase X_{An} in the calibration dataset is summarized in Supplementary Fig. 2A which is analogous to Fig. 2 in the main text.

Test data (n = 36) to independently verify regression quality were sourced from studies on H_2O-poor oceanic and continental tholeiites at range of pressures (0.1–1000 MPa). Specifically, data were sourced from experiments on MORBs (Grove et al., 1992; Yang et al., 1996) and continental tholeiites from Snake River Plain (Whitaker et al., 2007, 2008). The distribution of plagioclase X_{An} in the test dataset is summarized in Supplementary Fig. 2B which is analogous to Fig. 2B in the main text.

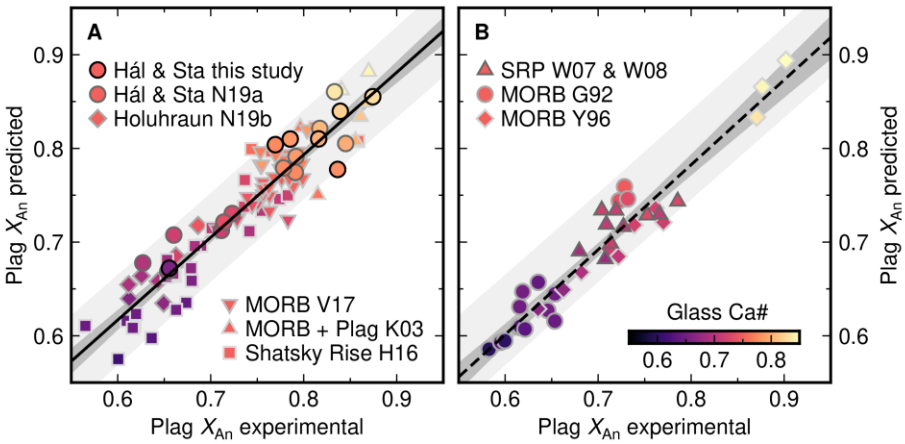

Supplementary Figure 2 (A) Performance of the multiple linear regression (Eq 1) used to predict plagioclase (plag) anorthite content (X_{An}, where X_{An} = molar Ca/(Ca+Na+K)) as a function melt composition. The black line shows a regression through calibration data from experimental studies on basalts from an ocean island, mid-ocean ridges and an oceanic plateau. Dark and pale grey envelopes show 95% confidence and prediction intervals, respectively. Data sources: N19a, ocean island basalts (OIBs) from Holuhraun in Iceland (Neave et al., 2019a); this study, OIBs from Háleyjabunga (Hál) and Stapafell (Sta) in Iceland at 100 and 600 MPa N19b, OIBs from Háleyjabunga (Hál) and Stapafell (Sta) in Iceland at 300 MPa (Neave et al., 2019b); V17, mid-ocean-ridge basalt (MORB) (Voigt et al., 2017); plagioclase-saturated MORB (Kohut and Nielsen, 2003); and oceanic plateau basalts from Shatsky Rise (Husen et al., 2016). (B) Performance of Eq 1 on test data from mid-ocean ridges and a continental hotspot. The dashed black line and dark grey envelope show a regression through the test data and its 95% confidence interval, respectively; the pale grey envelope shows the 95% prediction interval of Eq 1. Data sources: MORB (Grove et al., 1992; Yang et al., 1996); and continental tholeiites from Snake River Plain (SRP) (Whitaker et al., 2007, 2008).

Regression strategy

Least-squares multiple linear regression was then performed using the lm() function in R (R Development Core Team, 2016). The regression equation was selected by trial and error (e.g., Putirka, 2008). Namely, melt compositional parameters were variably combined and both overall r^2 values and p-values of individual regression parameters were evaluated until the following equation was identified (1σ values of regression coefficients are given in parentheses):

$$X_{An} = 0.92(0.07)\cdot Ca\#_{melt} + 1.63(0.24)\cdot Al\#_{melt} + 0.24(0.05)\cdot(\text{molar Ca/Al})_{melt} - 0.54(0.06), \quad (1)$$

where Ca# = molar Ca/(Ca+Na) and Al# = molar Al/(Al+Si). All regression coefficients are highly significant ($p < 0.001$), and the regression is robust ($r^2 = 0.88$; standard error = 0.025). Adding further compositional parameters such as melt MgO or K_2O contents did not improve the quality of the fit. The standard error of our new model (0.025) is considerably better than the standard errors of the models reviewed by Namur et al. (2012), which range from 0.044 to 0.090, though our model is only calibrated for oceanic basalts that are relatively poor in H_2O; the models of Namur et al. (2012) have comparable standard errors of ~0.030. Relationships between experimental X_{An}, predicted X_{An}, melt composition and other intrinsic conditions (pressure, temperature and oxygen fugacity) are summarized in Supplementary Fig. 3.

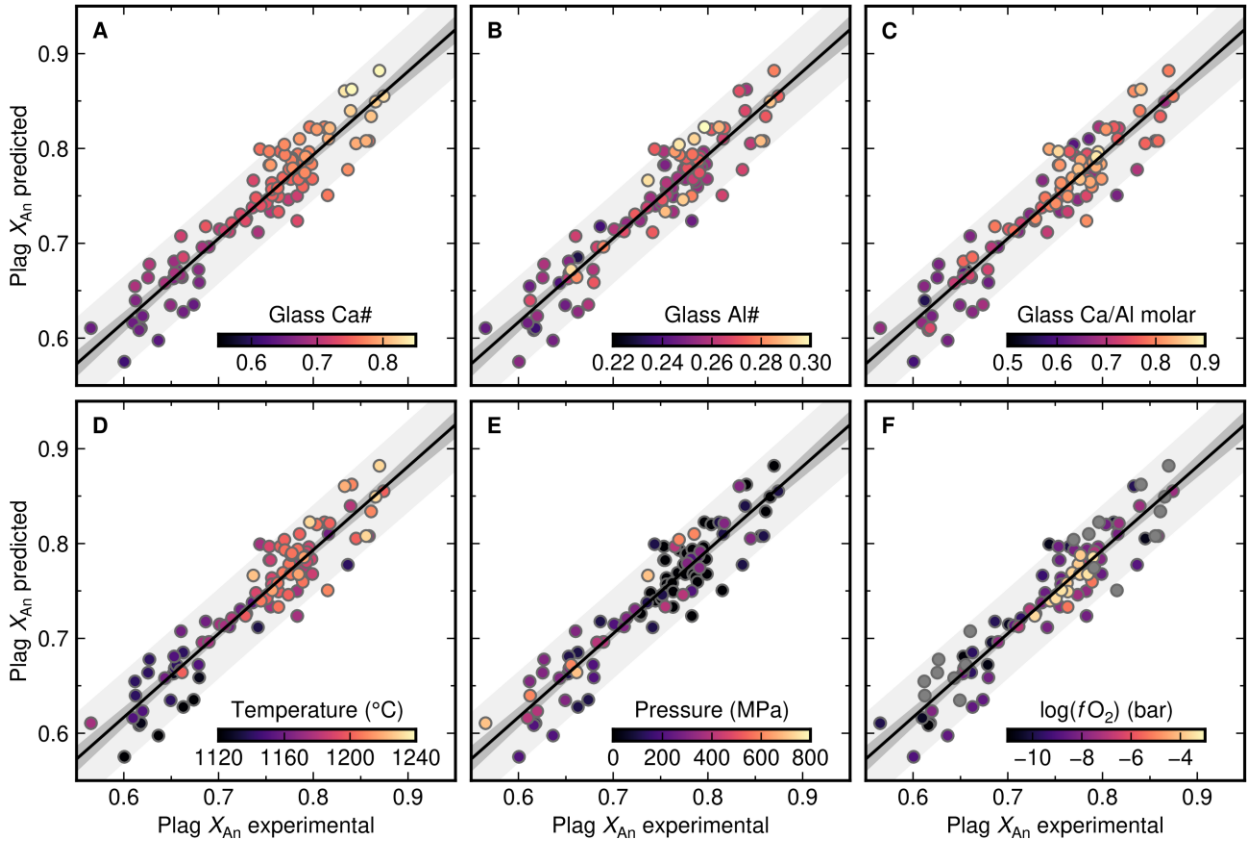

Supplementary Figure 3 Performance of the multiple linear regression (Eq 1) used to predict plagioclase (plag) anorthite content (X_{An}, where X_{An} = molar Ca/(Ca+Na+K)) as a function melt composition. The black line shows a regression through calibration data from experimental studies on basalts from an ocean island, mid-ocean ridges and an oceanic plateau and. Dark and pale grey envelopes show 95% confidence and prediction intervals, respectively. Data are colored as follows: (A) glass (i.e., melt) Ca#, where Ca# = molar Ca/(Ca+Na); (B) glass Al#, where Al# = molar Al/(Al+Si); (C) glass molar Ca/Al; (D) temperature; (E) pressure; and (F) oxygen fugacity (fO_2). Experiments for which fO_2 values were not reported are shown in grey.

While the strong dependence of predicted X_{An} on $Ca\#_{melt}$ is clear in Supplementary Fig. 3A, it is also important to note that experiments are well reproduced across a wide range of intrinsic conditions relevant to the evolution of oceanic basalts (Supplementary Figs 3D–3F). The possible underestimation of X_{An} in the coolest experiments is of little significance for our study that focusses on the significance of high-X_{An} plagioclase crystals.

A simple linear regression through the test data reveals a similarly strong relationship between experimental and predicted X_{An} as observed for the calibration data (r^2 = 0.92; standard error = 0.020). Moreover, relationships between experimental X_{An}, predicted X_{An}, melt composition and other intrinsic conditions in the test dataset are comparable to those in the calibration dataset (Supplementary Fig. 4). Importantly, Eq 1 reliably captures the high-X_{An} compositions reported from some experiments.

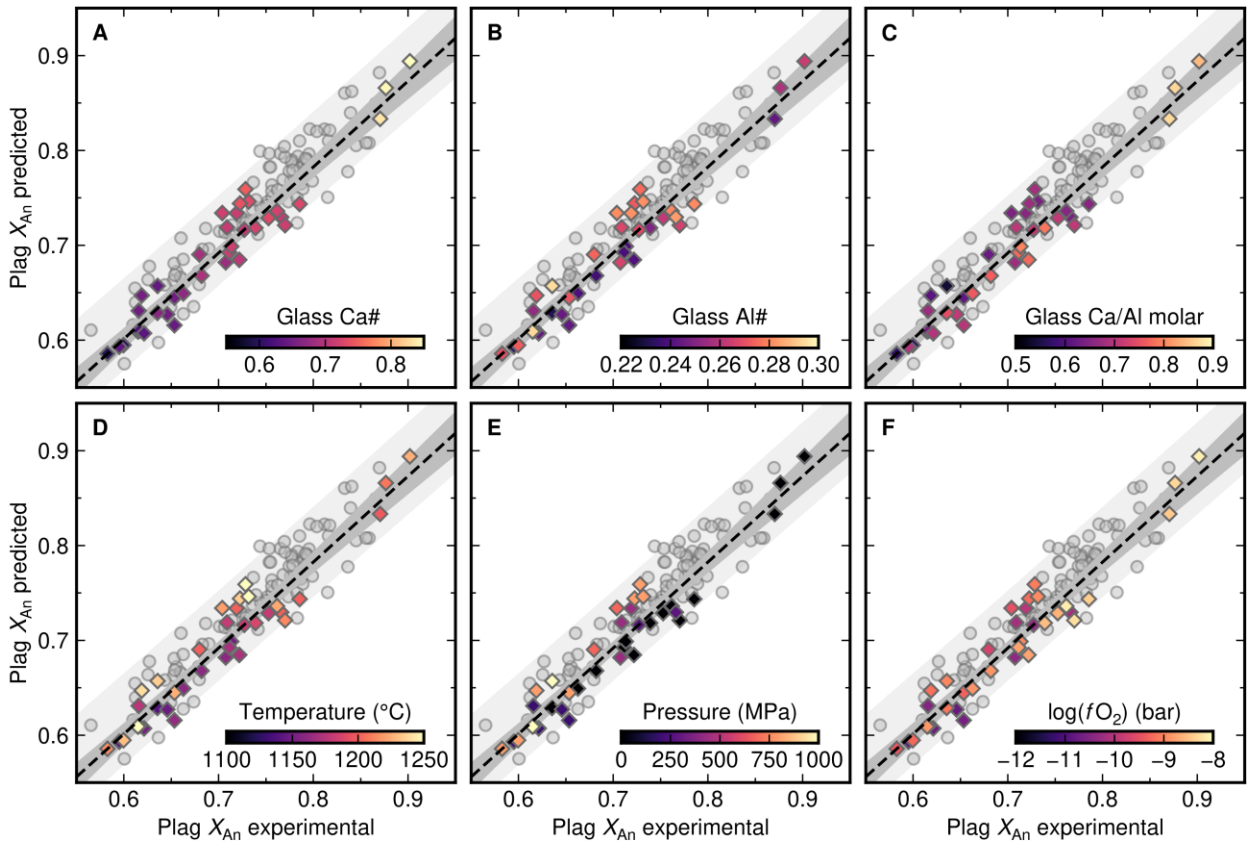

Supplementary Figure 4 Performance of Eq 1 on test data from mid-ocean ridges and a continental hotspot. The dashed black line and dark grey envelope show a regression through the test data and its 95% confidence interval, respectively; the pale grey envelope shows the 95% prediction interval of Eq 1. Regression and test data are respectively shown as grey circles and diamonds colored as follows: (A) glass (i.e., melt) Ca#, where Ca# = molar Ca/(Ca+Na); (B) glass Al#, where Al# = molar Al/(Al+Si); (C) glass molar Ca/Al; (D) temperature; (E) pressure; and (F) oxygen fugacity (fO_2).

Verifying plagioclase stability

Although Eq 1 can reliably predict the plagioclase X_{An} in equilibrium with oceanic basalts, it does not account for plagioclase stability. That is, it will return metastable equilibrium plagioclase X_{An} values for melt compositions that are plagioclase undersaturated. Predicted values of plagioclase X_{An} were filtered for plagioclase stability using the following criterion from Gale et al. (2014):

$$K_{d\ An} \times An_{liq} + K_{d\ Ab} + Ab_{liq} = 1. \quad (2)$$

Values of An_{liq} and Ab_{liq} were determined from glass compositions while $K_{d\ An}$ and $K_{d\ Ab}$ were predicted from regressions analogous in form to Eq 1 (r^2 = 0.82 and 0.42, respectively). Natural glasses were then determined to be saturated in plagioclase if the value of Eq 2 was within the 95% confidence interval of values estimated from plagioclase-saturated experiments. That is, plagioclase was considered stable when Eq 2 returned 1.00±0.03, which allows some tolerance for both analytical and fitting uncertainties. As for predicting plagioclase-liquid equilibria we

favoured this empirical approach over using thermodynamic models such as the MELTS algorithm (Ghiorso and Sack, 1995) to avoid making potentially erroneous assumptions about crystallization conditions.

PLAGIOGLASE IN OCEANIC BASALTS AND THE OCEANIC CRUST

Data sources

High-X_{An} plagioclase crystals occur throughout the oceanic realm. They are often major constituents of basalts from ocean islands and slow- to intermediate-spreading mid-ocean ridges (Lange et al., 2013), as well as cumulates from ophiolites and the lower oceanic crust (Browning, 1982; Lissenberg et al., 2013). Here we collated data from diverse studies on oceanic samples that report high-X_{An}. We explicitly did not incorporate data from arc settings where elevated X_{An} contents likely result from elevated melt H_2O contents initially suppressing plagioclase crystallization (Sisson and Grove, 1993).

Mineral data are rarely reported in consistent ways between different studies. For example, some studies only report macrocryst (i.e., phenocryst) compositions while others also consider microcryst and groundmass compositions; some separate core and rim analyses while others provide no textural information. In order to maximize our collated data of natural oceanic plagioclase compositions we therefore collated all available data, texturally constrained or not. Sources of natural plagioclase compositions are summarized in Supplementary Table 1.

Setting	Location	Sources	*n*
OIB	Iceland, Eastern Volcanic Zone	Passmore (2009), Neave et al. (2013), Neave et al. (2014) and Caracciolo et al. (2020)	2166
OIB	Iceland, Northern Volcanic Zone	Maclennan et al. (2003)	373
OIB	Galápagos	Cullen et al. (1989) and Stock et al. (2020)	974
OIB	Réunion	Valer et al. (2017)	14
OIB	Kerguelen	Annell et al. (2007)	20
MORB	Mid-Atlantic Ridge	Lange et al. (2013)	299
MORB	Southwest Indian Ridge	Lange et al. (2013)	383
MORB	Juan de Fuca Ridge	Lange et al. (2013)	68
MORB	Gakkel Ridge	Lange et al. (2013) and Bennett et al. (2019)	3969
Ophiolite	Samail Ophiolite, Oman	Browning (1982) and Koga et al. (2001)	98
Lower oceanic crust	East Pacific Rise	Constantin et al. (1996), Lissenberg et al. (2013) and Faak and Gillis (2016)	318
Lower oceanic crust	Southwest Indian Ridge	Dick et al. (2002)	7894

Supplementary Table 1 Sources of natural plagioclase data summarized in Fig. 4

REFERENCES CITED

Annell, H., Scoates, J.S., Weis, D., and Giret, A., 2007, Petrology of flood basalts at the tholeiitic-alkalic transition and phenocryst compositions, Mt. Marion Dufresne, Kerguelen Archipelago, Southern Indian Ocean: Canadian Mineralogist, v. 45, p. 809–835, doi:10.2113/gscanmin.45.4.809.

Barr, J.A., and Grove, T.L., 2010, AuPdFe ternary solution model and applications to understanding the fO_2 of hydrous, high-pressure experiments: Contributions to Mineralogy and Petrology, v. 160, p. 631–643, doi:10.1007/s00410-010-0497-z.

Bennett, E.N., Lissenberg, C.J., and Cashman, K. V., 2019, The significance of plagioclase textures in mid-ocean ridge basalt (Gakkel Ridge, Arctic Ocean): Contributions to Mineralogy and Petrology, v. 174, p. 49, doi:10.1007/s00410-019-1587-1.

Browning, P., 1982, The petrology, geochemistry and structure of the plutonic rocks of the Oman ophiolite: Open University, 404 p., doi:10.21954/ou.ro.0000de14.

Caracciolo, A., Bali, E., Guðfinnsson, G.H., Kahl, M., Halldórsson, A., Hartley, M.E., and Gunnarsson, H., 2020, Temporal evolution of magma and crystal mush storage conditions in the Bárðarbunga-Veiðivötn volcanic system, Iceland: Lithos, p. 105234, doi:10.1016/j.lithos.2019.105234.

Condomines, M., Grönvold, K., Hooker, P.J., Muehlenbachs, K., O'Nions, R.K., Óskarsson, N., and Oxburgh, E.R., 1983, Helium, oxygen, strontium and neodymium isotopic relationships in Icelandic volcanics: Earth and Planetary Science Letters, v. 66, p. 125–136, doi:10.1016/0012-821X(83)90131-0.

Constantin, M., Hékinian, R., Bideau, D., and Hébert, R., 1996, Construction of the oceanic lithosphere by magmatic intrusions: Petrological evidence from plutonic rocks formed along the fast-spreading East Pacific Rise: Geology, v. 24, p. 731–734, doi:10.1130/0091-7613(1996)024<0731:COTOLB>2.3.CO;2.

Cullen, A., Vicenzi, E.P., and McBirney, A.R., 1989, Plagioclase-ultraphyric basalts of the Galapagos archipelago: Journal of Volcanology and Geothermal Research, v. 37, p. 325–337, doi:10.1016/0377-0273(89)90087-5.

Dick, H.J.B. et al., 2002, Primary silicate mineral chemistry of a 1.5-km section of very slow spreading lower ocean crust: ODP Hole 735B, Southwest Indian Ridge: Proceedings of the Ocean Drilling Program, Scientific Results, v. 176, doi:10.2973/odp.proc.sr.176.001.2002.

Faak, K., and Gillis, K.M., 2016, Slow cooling of the lowermost oceanic crust at the fast-spreading East Pacific Rise: Geology, v. 44, p. G37353.1, doi:10.1130/G37353.1.

Gaetani, G.A., and Grove, T.L., 1998, The influence of water on melting of mantle peridotite: Contributions to Mineralogy and Petrology, v. 131, p. 323–346, doi:10.1007/s004100050396.

Gale, A., Langmuir, C.H., and Dalton, C.A., 2014, The Global Systematics of Ocean Ridge Basalts and their Origin: Journal of Petrology, v. 55, p. 1051–1082, doi:10.1093/petrology/egu017.

Ghiorso, M.S., and Sack, R.O., 1995, Chemical mass transfer in magmatic processes IV. A revised and internally consistent thermodynamic model for the interpolation and extrapolation of liquid-solid equilibria in magmatic systems at elevated temperatures and

pressures: Contributions to Mineralogy and Petrology, v. 119, p. 197–212, doi:10.1007/BF00307281.

Grove, T.L., Kinzler, R.J., and Bryan, W.B., 1992, Fractionation of Mid-Ocean Ridge Basalt (MORB), *in* Mantle Flow and Melt Generation at Mid-Ocean Ridges, Geophysical Monograph 71, Washington D.C., American Geophysical Union, p. 281–310.

Gurenko, A.A., and Chaussidon, M., 1995, Enriched and depleted primitive melts included in olivine from Icelandic tholeiites: Origin by continuous melting of a single mantle column: Geochimica et Cosmochimica Acta, v. 59, p. 2905–2917, doi:10.1016/0016-7037(95)00184-0.

Husen, A., Almeev, R.R., and Holtz, F., 2016, The Effect of H_2O and Pressure on Multiple Saturation and Liquid Lines of Descent in Basalt from the Shatsky Rise: Journal of Petrology, v. 57, p. 309–344, doi:10.1093/petrology/egw008.

Jarosewich, E., Gooley, R., and Husler, J., 1987, Chromium Augite - A New Microprobe Reference Sample: Geostandards and Geoanalytical Research, v. 11, p. 197–198, doi:10.1111/j.1751-908X.1987.tb00027.x.

Jarosewich, E., Nelen, J.A., and Norberg, J.A., 1980, Reference samples for electron microprobe analysis: Geostandards Newsletter, v. 4, p. 43–47.

Koga, K.T., Kelemen, P.B., and Shimizu, N., 2001, Petrogenesis of the crust-mantle transition zone and the origin of lower crustal wehrlite in the Oman ophiolite: Geochemistry, Geophysics, Geosystems, v. 2, doi:10.1029/2000GC000132.

Kohut, E.J., and Nielsen, R.L., 2003, Low-pressure phase equilibria of anhydrous anorthite-bearing mafic magmas: Geochemistry, Geophysics, Geosystems, v. 4, p. 1–27, doi:10.1029/2002GC000451.

Kress, V.C., and Carmichael, I.S.E., 1991, The compressibility of silicate liquids containing Fe_2O_3 and the effect of composition, temperature, oxygen fugacity and pressure on their redox states: Contributions to Mineralogy and Petrology, v. 108, p. 82–92, doi:10.1007/BF00307328.

Lange, A.E., Nielsen, R.L., Tepley, F.J., and Kent, A.J.R., 2013, The petrogenesis of plagioclase-phyric basalts at mid-ocean ridges: Geochemistry, Geophysics, Geosystems, v. 14, p. 3282–3296, doi:10.1002/ggge.20207.

Lissenberg, C.J., MacLeod, C.J., Howard, K.A., and Godard, M., 2013, Pervasive reactive melt migration through fast-spreading lower oceanic crust (Hess Deep, equatorial Pacific Ocean): Earth and Planetary Science Letters, v. 361, p. 436–447, doi:10.1016/j.epsl.2012.11.012.

Maclennan, J., 2008, Lead isotope variability in olivine-hosted melt inclusions from Iceland: Geochimica et Cosmochimica Acta, v. 72, p. 4159–4176, doi:10.1016/j.gca.2008.05.034.

Maclennan, J., McKenzie, D., Grönvold, K., Shimizu, N., Eiler, J.M., and Kitchen, N., 2003, Melt mixing and crystallization under Theistareykir, northeast Iceland: Geochemistry, Geophysics, Geosystems, v. 4, p. 1–40, doi:10.1029/2003GC000558.

Namur, O., Charlier, B., Toplis, M.J., and Vander Auwera, J., 2012, Prediction of plagioclase-melt equilibria in anhydrous silicate melts at 1-atm: Contributions to Mineralogy and Petrology, v. 163, p. 133–150, doi:10.1007/s00410-011-0662-z.

Neave, D.A., Bali, E., Guðfinnsson, G.H., Halldórsson, S.A., Kahl, M., Schmidt, A.-S., and Holtz, F., 2019a, Clinopyroxene–liquid equilibria and geothermobarometry in natural and experimental tholeiites: the 2014–2015 Holuhraun eruption, Iceland: Journal of Petrology, v. 60, p. 1653–1680, doi:10.1093/petrology/egz042.

Neave, D.A., Maclennan, J., Hartley, M.E., Edmonds, M., and Thordarson, T., 2014, Crystal storage and transfer in basaltic systems: the Skuggafjöll eruption, Iceland: Journal of Petrology, v. 55, p. 2311–2346, doi:10.1093/petrology/egu058.

Neave, D.A., Namur, O., Shorttle, O., and Holtz, F., 2019b, Magmatic evolution biases basaltic records of mantle chemistry towards melts from recycled sources: Earth and Planetary Science Letters, v. 520, p. 199–211, doi:10.1016/j.epsl.2019.06.003.

Neave, D.A., Passmore, E., Maclennan, J., Fitton, J.G., and Thordarson, T., 2013, Crystal-melt relationships and the record of deep mixing and crystallization in the AD 1783 Laki eruption, Iceland: Journal of Petrology, v. 54, p. 1661–1690, doi:10.1093/petrology/egt027.

Neave, D.A., Shorttle, O., Oeser, M., Weyer, S., and Kobayashi, K., 2018, Mantle-derived trace element variability in olivines and their melt inclusions: Earth and Planetary Science Letters, v. 483, p. 90–104, doi:10.1016/j.epsl.2017.12.014.

Passmore, E., 2009, Feeding large eruptions: crystallisation, mixing and degassing in Icelandic magma chambers: University of Edinburgh, 379 p.

Peate, D.W., Baker, J.A., Jakobsson, S.P., Waight, T.E., Kent, A.J.R., Grassineau, N. V., and Skovgaard, A.C., 2009, Historic magmatism on the Reykjanes Peninsula, Iceland: A snap-shot of melt generation at a ridge segment: Contributions to Mineralogy and Petrology, v. 157, p. 359–382, doi:10.1007/s00410-008-0339-4.

Putirka, K.D., 2008, Thermometers and Barometers for Volcanic Systems: Reviews in Mineralogy and Geochemistry, v. 69, p. 61–120, doi:10.2138/rmg.2008.69.3.

R Development Core Team, 2016, R: A Language and Environment for Statistical Computing: R Foundation for Statistical Computing,.

Schuessler, J.A., Botcharnikov, R.E., Behrens, H., Misiti, V., and Freda, C., 2008, Oxidation state of iron in hydrous phono-tephritic melts: American Mineralogist, v. 93, p. 1493–1504, doi:10.2138/am.2008.2795.

Shorttle, O., and Maclennan, J., 2011, Compositional trends of Icelandic basalts: Implications for

short-length scale lithological heterogeneity in mantle plumes: Geochemistry, Geophysics, Geosystems, v. 12, p. 1–32, doi:10.1029/2011GC003748.

Sisson, T.W., and Grove, T.L., 1993, Experimental investigations of the role of H_2O in calc-alkaline differentiation and subduction zone magmatism: Contributions to Mineralogy and Petrology, v. 113, p. 143–166, doi:10.1007/BF00283225.

Stock, M.J., Howard, K.A., Geist, D., Neave, D.A., Buisman, I., Maclennan, J., Gleeson, M.L.M., and Bernard, B., 2020, Cryptic evolved melts beneath monotonous basaltic shield volcanoes in the Galápagos Archipelago: Nature Communications, v. 11, p. 3767, doi:10.1038/s41467-020-17590-x.

Valer, M., Bachèlery, P., and Schiano, P., 2017, The Petrogenesis of Plagioclase-ultraphyric Basalts from La Réunion Island: Journal of Petrology, p. 1–24, doi:10.1093/petrology/egx030.

Voigt, M., Coogan, L.A., and von der Handt, A., 2017, Experimental investigation of the stability of clinopyroxene in mid-ocean ridge basalts: The role of Cr and Ca/Al: Lithos, v. 274–275, p. 240–253, doi:10.1016/j.lithos.2017.01.003.

Whitaker, M.L., Nekvasil, H., Lindsley, D.H., and Difrancesco, N.J., 2007, The role of pressure in producing compositional diversity in intraplate basaltic magmas: Journal of Petrology, v. 48, p. 365–393, doi:10.1093/petrology/egl063.

Whitaker, M.L., Nekvasil, H., Lindsley, D.H., and McCurry, M., 2008, Can crystallization of olivine tholeiite give rise to potassic rhyolites? - An experimental investigation: Bulletin of Volcanology, v. 70, p. 417–434, doi:10.1007/s00445-007-0146-1.

Yang, H.-J., Kinzler, R.J., and Grove, T.L., 1996, Experiments and models of anhydrous, basaltic olivine-plagioclase-augite saturated melts from 0.001 to 10 kbar: Contributions to Mineralogy and Petrology, v. 124, p. 1–18, doi:10.1007/s004100050169.